Emergent quasiperiodicity from polariton-phonon hybrid excitations in waveguide quantum optomechanics

Han-Jie Zhu,[1] Lin Zhuang,[2,*] Xiao-Ming Zhao,[3] Jin-Kui Zhao,[1,4] Jian-Jun Zhang,[1,4] Guo-Feng Zhang,[5] and Wu-Ming Liu[1,6,4]

[1]*Beijing National Laboratory for Condensed Matter Physics, Institute of Physics, Chinese Academy of Sciences, Beijing 100190, China*
[2]*State Key Laboratory of Optoelectronic Materials and Technologies, School of Physics, Sun Yat-Sen University, Guangzhou 510275, China*
[3]*Department of Physics and Institute of Theoretical Physics, University of Science and Technology Beijing, Beijing 100083, China*
[4]*Songshan Lake Materials Laboratory, Dongguan, Guangdong 523808, China*
[5]*School of Physics, Beihang University, Beijing 100191, China*
[6]*School of Physical Sciences, University of Chinese Academy of Sciences, Beijing 100190, China*

(Received 18 July 2022; revised 25 March 2024; accepted 26 March 2024; published 9 April 2024)

We investigate polariton-phonon hybrid excitations, which describe the collective excitations of emitter-photon polaritons and vibrational phonons, in a periodic array of vibrating two-level emitters interacting with waveguide photons. These excitations present unexpected features in the subradiant regime, including the appearance of topological edge states and transitions between ergodic and multifractal excitations. We reveal that these features are attributed to the emergence of a phonon-induced quasiperiodic structure, where phonons can effectively create a periodic potential that is incommensurate with the emitter lattice. A possible realization consisting of an array of laser-cooled atoms trapped near an optical nanofiber is also proposed. Our results demonstrate the possibility of utilizing vibrations as a unique degree of freedom in the exploration of many-body physics with waveguide quantum electrodynamics systems.

DOI: 10.1103/PhysRevB.109.165419

I. INTRODUCTION

Waveguide quantum electrodynamics (QED), an emerging field focusing on the interaction of propagating waveguide photons with quantum emitters, has attracted intense interest in recent years motivated by the significant progresses in quantum technologies [1–5]. In addition to applications in quantum networks and quantum computation, waveguide QED also provides a promising platform for quantum simulation of many-body physics. A remarkable advantage of waveguide QED systems is that they can exhibit strong light-matter interactions and long-range couplings between emitters mediated by waveguide photons [6–9]. These features allow the exploration of a variety of many-body phenomena that were previously difficult to generate in other platforms, including unconventional topological phases [10–12], superradiant and subradiant states [13–18], and peculiar correlations between photons [19–22].

While emitters are assumed to be static in most waveguide QED studies, their mechanical motions can act as unique degrees of freedom due to the position-dependent nature of light-matter interactions [23,24]. In particular, the vibrational degrees of freedom, which arise naturally in cold-atom experiments [25], can contribute to interesting phenomena even in small systems with few emitters [26–28]. In the many-body regime (many emitters), the collective excitations of emitters and photons (polaritons) follow unconventional dispersion relations and exhibit peculiar effects ranging from fermionization to quantum chaos [29–36]. These polaritons can propagate along the waveguide and interact with lattice vibrations, thus the resulting hybrid excitations may behave quite differently compared to the bare polaritons. We can expect the emergence of highly interesting many-body phenomena as a result of the interplay between waveguide polaritons and vibrational phonons. Nevertheless, the physics arising from the polariton-phonon interactions remains largely unexplored in waveguide QEDs due to the complexity from the hybridization of photons, emitters, and phonons, as well as the long-range nature of the photon-mediated interactions.

In this paper, we develop a description of polariton-phonon hybrid excitations in an array of vibrating emitters coupled to a waveguide. We find that these excitations exhibit a distinctly different behavior compared to bare polaritons in a subwavelength finite array. We then identify the emergence of an effective quasiperiodic potential, induced by the combination of phonon scattering and waveguide-mediated long-range couplings, as the key element behind the intriguing behavior of hybrid excitations. This quasiperiodicity splits the originally continuous spectrum into a set of bands and gives rise to topological edge states inside the band gaps. In addition, due to the quasiperiodicity, the subradiant excitations experience an ergodic-multifractal transition with an edge separating the spectrum into two regions. We also propose a cold-atom based scheme for the realization and detection of hybrid excitations in experiments.

II. COUPLING WAVEGUIDE POLARITONS WITH PHONONS

We consider a periodic array of N traps along a one-dimensional waveguide, each loaded with a two-level emitter,

*Corresponding author: stszhl@mail.sysu.edu.cn

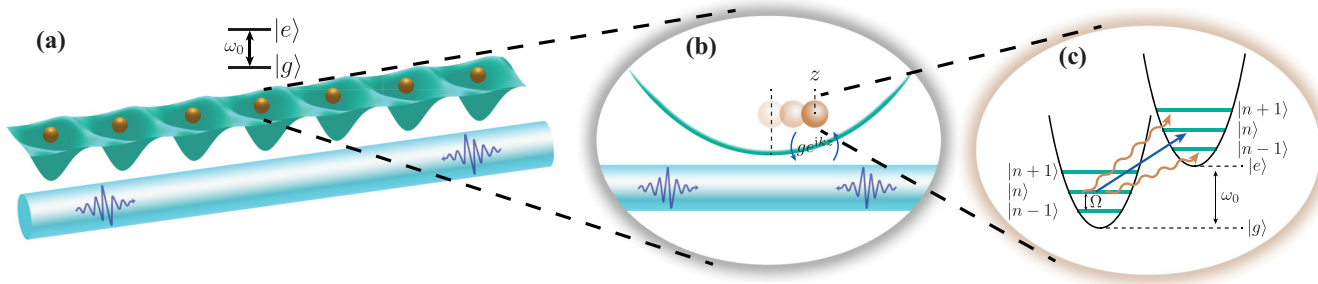

FIG. 1. Schematic of the waveguide QED setup with vibrating emitters. (a) A periodic array of emitters is trapped near a waveguide. The internal degrees of freedom of each emitter can be described by a two-level system with ground state $|g\rangle$, excited state $|e\rangle$, and resonance frequency ω_0. (b) Each lattice site can be viewed as a parabolic potential and allows the emitter to vibrate parallel to the waveguide with phonon energy Ω. The emitters interact with waveguide photons via an electric dipole interaction whose strength ge^{ikz} is position dependent and is proportional to the amplitude of the electric field at the emitter position z. (c) This interaction leads to the transitions between $|g\rangle$ and $|e\rangle$ of emitters with different vibrational quantum numbers, thus mixing phonons with emitters and photons.

as depicted in Fig. 1. The emitters strongly radiate into the waveguide and are allowed to vibrate parallel to the waveguide. The absorption or emission of waveguide photons by emitters can lead to the deformation of the array structure, and thus excite the vibrational modes (phonons). The system is characterized by [26]

$$\mathcal{H} = \sum_k \omega_k b_k^\dagger b_k + \sum_m \omega_0 \sigma_m^\dagger \sigma_m + \sum_m \Omega a_m^\dagger a_m + \frac{g}{\sqrt{L}} \sum_{k,m} (\sigma_m^\dagger b_k e^{ik\hat{z}_m} + \sigma_m b_k^\dagger e^{-ik\hat{z}_m}), \quad (1)$$

where b_k, σ_m, and a_m are the annihilation operators of the waveguide photon, emitter excitation, and phonon of the mth site, respectively. Here, $\omega_k = c|k|$ is the frequency of the photon with wave vector k, where c is the light speed in the waveguide. The resonance frequencies of the emitters and vibrational modes are given by ω_0 and Ω, respectively. Parameter g is the atom-light interaction strength, L is the normalization length, and $\hat{z}_m = z_m + u_0\hat{x}_m$ is the position operator where z_m is the equilibrium position of the mth atom, u_0 is the quantum of the vibrational mode, and $\hat{x}_m = a_m^\dagger + a_m$. Instead of a few-emitter cases, we focus on the many-body regime ($N \gg 1$) where emitters and photons form polaritons with strong collective superradiant and subradiant behavior.

In the Markovian approximation, photons can be integrated out [37,38] and the system is described by the effective Hamiltonian $H = H_0 + H_p + H_I$, where $H_0 = -i\Gamma_0 \sum_{m,n} e^{i\varphi|m-n|}\sigma_m^\dagger\sigma_n/2$ and $H_p = \sum_m \Omega a_m^\dagger a_m$ are the Hamiltonians of emitters and phonons, respectively, and

$$H_I = -i\frac{\Gamma_0}{2} \sum_{m,n} e^{i\varphi|m-n| + i\eta\,\mathrm{sign}(m-n)(\hat{x}_m - \hat{x}_n)} \sigma_m^\dagger \sigma_n - H_0, \quad (2)$$

where $\Gamma_0 = 2g^2/c$ is the decay rate for a single emitter into the waveguide, the phase $\varphi \equiv k_0 d \,(\mathrm{mod}\, 2\pi)$ is determined by the wave number $k_0 = \omega_0/c$ and the spacing d between adjacent emitters, and $\eta = k_0 u_0$ is the relative optomechanical coupling. The emitter excitation number $\mathcal{N} = \sum_m \sigma_m^\dagger \sigma_m$ is conserved in H, thus the Hamiltonian can be projected to subspaces with fixed $\mathcal{N}$, where the free Hamiltonian of atoms $\sum_m \omega_0 \sigma_m^\dagger \sigma_m$ produces constant energy and can be discarded. We restrict ourselves to the Lamb-Dicke regime $\eta\langle\hat{x}_m^2\rangle^{1/2} \ll 1$, where the mechanical fluctuations are small enough compared to the atomic spacing, i.e., $u_0\langle\hat{x}_m^2\rangle^{1/2} \ll d$. In this regime, the single-phonon process is dominant, thus we can neglect processes where multiple phonons are simultaneously absorbed or emitted [39–42].

We first consider an infinite array ($N \to \infty$) which is invariant under lattice translations. Without phonons, the single-excitation eigenstates are light-matter excitations (polaritons) $|k\rangle = \sigma_k^\dagger|0\rangle = N^{-1/2}\sum_m e^{ikz_m}\sigma_m^\dagger|0\rangle$ with quasimomentum k [6,29]. The states $|\pm k_0\rangle$ emit photons superradiantly to the waveguide and are marked by a large imaginary eigenvalue $-iN\Gamma_0/4$, while the remaining $N-2$ states are dark with zero decay rate. The energy dispersion of dark states is given by $\varepsilon_k = (\Gamma_0/4)\sum_{\epsilon=\pm}\cot[(k_0+\epsilon k)d/2]$. Its curve is split into upper and lower branches separated by a gap.

III. THE EMERGENCE OF POLARITON-PHONON HYBRID EXCITATIONS

In the presence of atom-phonon interactions, polaritons and phonons are coupled to each other and form polariton-phonon hybrid excitations. The dressing effects of phonons can lead to nontrivial phenomena in finite arrays. In Fig. 2(a), we plot the energy spectrum of the lower excitation branch obtained by exact diagonalization. We find that the spectrum of hybrid excitations deviates significantly from the bare polaritons. Its subradiant part shows irregular characters, and a group of near-degenerate states separated from the spectrum branch can be identified.

To investigate phonon effects in longer arrays, we decouple polaritons from phonons via the Schrieffer-Wolff transformation (SWT) [43,44]. An effective Hamiltonian $H' = P_0 e^S H e^{-S} P_0$ can be obtained by choosing a proper operator S to eliminate the polariton-phonon coupling to the first order, where P_0 is the projector onto the single-polariton subspace without phonons (Appendix A). In finite arrays, dark states become subradiant and possess complex eigenvalues. The discrepancy in their decay rates creates an imaginary energy gap separating the single-polariton subspace without phonons from the rest of the spectrum. This feature allows the decoupling of emitters from phonons as long as the coupling

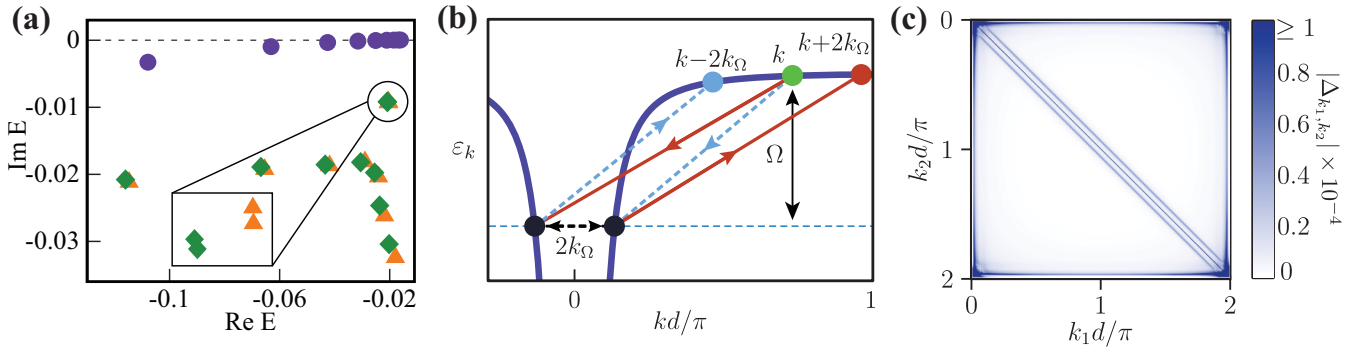

FIG. 2. (a) Subradiant part of the complex single-excitation spectrum obtained from the Schrieffer-Wolff transformation (orange triangle) in comparison with the exact diagonalization results (green diamond) and the single-polariton spectrum (blue circle). The inset shows the detailed structure of the near-degenerate group in spectrum. The calculation has been performed for an array of $N = 12$ emitters with $\Gamma_0 = \Omega = 1$ and $\eta = \varphi = \pi/50$. (b) Lower branch of the single-polariton dispersion. Phonons can mediate effective interactions between polaritons with quasi-momentum change $\pm 2k_\Omega$. (c) Color map of the phonon correction Δ in k space. The calculation has been performed for $10\Gamma_0 = \Omega = 1$, $\varphi = 0.06$, $\eta/\varphi = 1$, and $N = 240$.

is much smaller than the energy gap. In the limit of large N, this is equivalent to $\eta^2\varphi^{-1}(\Gamma_0/\Omega)^3 \ll N^{-1}$. This condition can always be satisfied in the weak coupling regime $\eta \ll 1$ by adjusting the decay rate Γ_0 and the atomic spacing d, which are highly tunable in experiments. More details about the validity of SWT can be found in Appendix A. In Fig. 2(a), we demonstrate the accuracy of SWT by comparing the energy spectra obtained from H' with the exact diagonalization results. Here a satisfactory agreement is obtained between the two methods.

In Figs. 3(a) and 3(e), we present the excitation spectrum in a longer array, where its most subradiant part splits into narrow bands with the increase of η, as opposed to the original polariton spectrum which is continuous and composed of delocalized Bloch states. For each normalized eigenstate $|\psi\rangle = \sum_n \psi_n|n\rangle$, we calculate its inverse participation ratio (IPR) as a measure of localization, which is defined as IPR $= \sum_n |\psi_n|^4$ and crosses from N^{-1} in the completely delocalized regime to 1 in the localized situation. The spectrum consists of different types of excitations with diverse spatial distribution, as shown in Figs. 3(b)–3(d). Compared to the delocalized states in the continuous band [Fig. 3(d)], states in the narrow bands become spatially modulated [Fig. 3(b)]. Moreover, we identify degenerate pairs of edge states which are highly localized at the boundaries [Fig. 3(c)]. These features indicate that the subradiant excitations are significantly modified by phonons in the finite arrays.

IV. PHONON-INDUCED QUASIPERIODICITY

Our central objective is to identify the mechanism responsible for these intriguing behaviors. Therefore, we consider a finite array in the $\varphi \ll 1$ limit and focus on the subradiant states on the lower excitation branch. The subradiant states in infinite arrays with energy E_k can be approximated by $|\Psi_k\rangle = |k, 0\rangle + \sum_p A_k(p)|k-p, p\rangle$, where $|k, 0\rangle = \sigma_k^\dagger|0\rangle$ and $|k, p\rangle = \sigma_k^\dagger a_p^\dagger|0\rangle$ are Bloch states without and with phonons, respectively. Here the wave function is truncated at the single-phonon level since single-phonon processes play a primary role within the Lamb-Dicke regime. $A_k(p)$ has two peaks at $p = k \pm k_\Omega$, which correspond to the resonant phonon processes connecting $|k, 0\rangle$ to $|\mp k_\Omega, k \pm k_\Omega\rangle$, respectively, where $k_\Omega > 0$ is determined by $\varepsilon_k = \Omega + \varepsilon_{k_\Omega}$. By acting H on this state, we obtain the eigenvalue relation $H|\Psi_k\rangle = E_k|\Psi_k\rangle - i\Gamma_0\delta_k/2$, where δ_k is the boundary term:

$$\delta_k = \delta_{k,0} + \sum_{\pm} A_k(k \pm k_\Omega)\delta_{\mp k_\Omega, k\pm k_\Omega}. \tag{3}$$

Here $\delta_{k,0} = g_k|k_0, 0\rangle - h_k|-k_0, 0\rangle$ and $\delta_{\pm k_\Omega, k\mp k_\Omega} = g_{\pm k_\Omega}|k_0, k \mp k_\Omega\rangle - h_{\pm k_\Omega}|-k_0, k \mp k_\Omega\rangle$ describe the boundary effects on $|k, 0\rangle$ and $|\pm k_\Omega, k \mp k_\Omega\rangle$, respectively, and the coefficients are $g_k = e^{i(k-k_0)z_1}/[1 - e^{i(k-k_0)d}]$ and $h_k = e^{i(k+k_0)z_N}/[e^{-i(k+k_0)d} - 1]$. In this eigenvalue relation, we account for the boundary effects of H_0 only since the emitter-phonon couplings create much smaller boundary effects. Similarly, the contributions from the single-phonon states are also neglected except for $|\pm k_\Omega, k \mp k_\Omega\rangle$. The boundary term δ_k can be canceled by the linear combination of $|k, 0\rangle$ and $|-k, 0\rangle$, and this procedure provides the correct eigenstate $g_{-k}|k, 0\rangle - g_k|-k, 0\rangle$ in the absence of atom-phonon coupling, where the wave number is given by the equation $g_k h_{-k} = g_{-k}h_k$ [29]. To cancel $\delta_{\pm k_\Omega, k\mp k_\Omega}$, we notice that k_Ω behaves almost as a constant and can be approximated by $k_\Omega d \approx (\varphi\Gamma_0/\Omega)^{1/2}$, as long as $|k\rangle$ remains in the quasiflat regime on the lower excitation branch, as shown in Fig. 2(b). This effectively induces a coupling between $|\Psi_k\rangle$ and $|\Psi_{k\pm 2k_\Omega}\rangle$.

Physically, this effective coupling can be understood as follows: Polaritons can be reflected from the boundaries in finite arrays. A polariton $|k, 0\rangle$ can be scattered into its resonant state $|\pm k_\Omega, k \mp k_\Omega\rangle$ and emits a phonon, while this state can be reflected into $|\mp k_\Omega, k \mp k_\Omega\rangle$, and finally scattered back into $|k \mp 2k_\Omega, 0\rangle$ after absorbing the phonon previously emitted, as shown in Fig. 2(b). This process effectively creates an interaction with momentum change $\mp 2k_\Omega$.

This momentum-change process plays a crucial role in the intriguing behavior of subradiant excitations. In the $\varphi \ll 1$ regime, we obtain an expression of $H' = H_0 + \Delta$, where the phonon-induced interactions Δ can be approximated as $\Delta \approx \sum_k [V_k(e^{-i\theta_k}|k\rangle\langle k + 2k_\Omega| + e^{i\theta_k}|k + 2k_\Omega\rangle\langle k|)/2 + \delta\varepsilon_k|k\rangle\langle k|]$. Here V_k is a complex effective coupling strength, θ_k is a phase factor, and $\delta\varepsilon_k$ accounts for the energy shift (Appendix B).

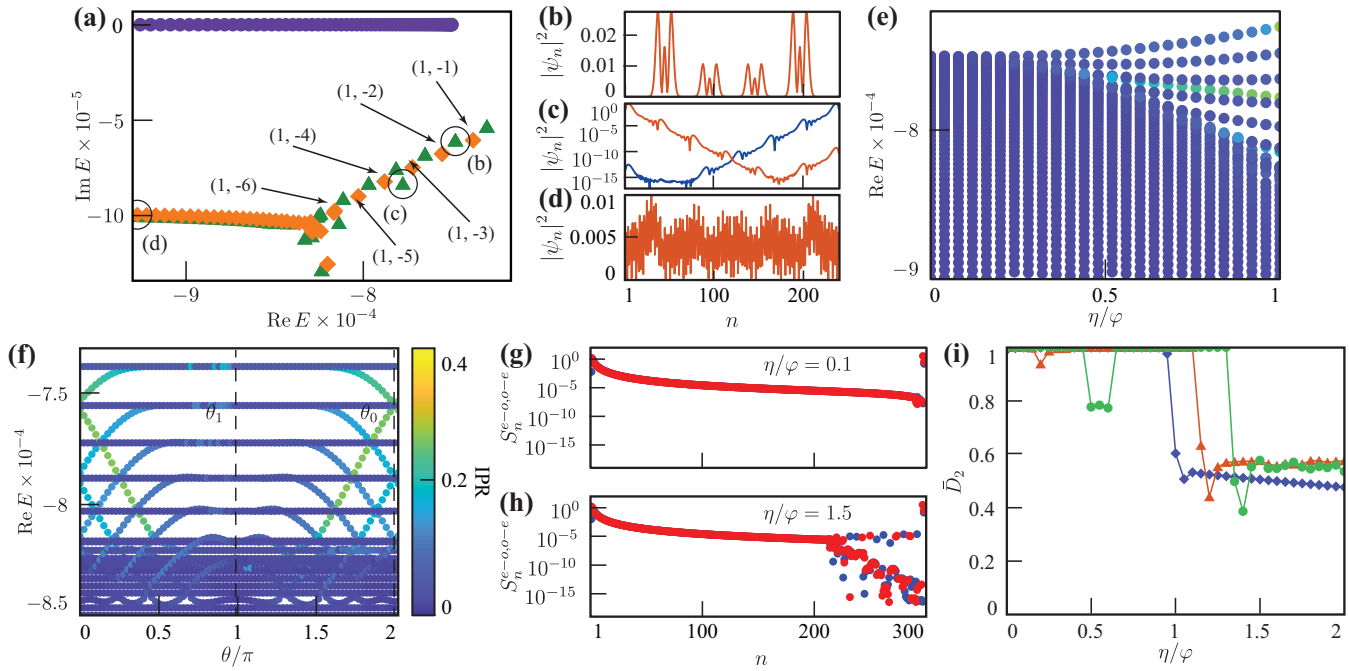

FIG. 3. (a) The most subradiant part of the complex single-excitation spectrum obtained from the effective Hamiltonian Eq. (4) (orange diamond) in comparison with the Schrieffer-Wolff transformation results (green triangle) and the single-polariton spectrum (blue circle). Topological invariants (μ, ν) for clearly observable spectral gaps are indicated. (b), (c), (d) The wave functions of three characteristic eigenstates corresponded to the states (b), (c), and (d) in spectrum (a), respectively. (e) Real spectrum of the most subradiant excitations as a function of the optomechanical coupling η. (f) Real spectrum of the most subradiant excitations in H_{eff} [Eq. (4)] with the same parameters in (a), as a function of the modulation phase θ. In real arrays, θ is fixed at discrete values $\theta_n = n\pi - \pi\beta(N+1) \bmod 2\pi$ due to the mirror symmetry inherited from the original Hamiltonian $\mathcal{H}$. (a)–(f) were generated for an array of $N = 240$ emitters with $10\Gamma_0 = \Omega = 1$, $\varphi = 0.03$ and $\eta/\varphi = 1$ [except in (e)]. (g), (h) Level spacing S_n^{e-o} (red) and S_n^{o-e} (blue) for the system with $\eta/\varphi = 0.1$ (g) and $\eta/\varphi = 1.5$ (h), respectively. (i), Mean fractal dimensions $\bar{D}_2$ for three subbands with the highest energy. Three highest subbands arranged in energy-descending order are labeled by blue diamond, red triangle, and green circle, respectively. (g)–(i) were generated for an array of $N = 600$ emitters with $10\Gamma_0 = \Omega = 1$ and $\varphi = 0.03$.

This can be verified in Fig. 2(c), where the main contributions to Δ come from $|k\rangle\langle k|$ and $|k\rangle\langle k \pm 2k_\Omega|$, which manifest themselves as the oblique lines parallel to the diagonal in the figure. All three coefficients change slowly in the quasiflat regime, thus H' can be further approximated by replacing three coefficients by their values at $k = \pi/d$. In real space, the resulting effective Hamiltonian can be written as

$$H' \approx H_{\text{eff}} = H_0 + V \sum_m \cos(2k_\Omega dm + \theta)|m\rangle\langle m|, \qquad (4)$$

which describes the original polaritons with an additional complex on-site potential being cosine modulated. Here V and θ serve as the amplitude and phase of the modulation, and take the values of V_k and θ_k at $k = \pi/d$, respectively (Appendix B). Meanwhile, we omit the near-constant energy shift ε_k. This effective Hamiltonian provides a qualitatively correct description of subradiant excitations, as shown in Fig. 3(a).

The on-site potential in H_{eff} [Eq. (4)] is, in general, incommensurate with the lattice since k_Ω is determined by the transcendental equation $\varepsilon_k = \Omega + \varepsilon_{k_\Omega}$. Therefore, H_{eff} can be regarded as a one-dimensional quasiperiodic model with long-range waveguide-mediated hoppings and a complex potential. This quasiperiodicity fundamentally changes the behavior of subradiant excitations. We notice that k_Ω can be approximated by $k_\Omega d/\pi \approx q^{-1}$, where $q \gg 1$ is an integer since $k_\Omega d/\pi \ll 1$. Thus, the quasiperiodicity naturally splits the spectrum into q bands in the first-order rational approximation, and the bands near the edge of the spectrum become much narrower. This explains the splitting of the spectrum in Figs. 3(a) and 3(e).

V. EDGE STATES AND ERGODIC-MULTIFRACTAL TRANSITIONS

Interestingly, the spectrum includes degenerate pairs of edge states localized over boundaries [Fig. 3(c)]. These states are topological edge states as a result of the quasiperiodicity. This is revealed through H_{eff}, which inherits the topological properties of its two-dimensional ancestor Hamiltonian $H_{2\text{D}} = \int_0^{2\pi} (d\theta/2\pi) H_{\text{eff}}(\theta)$. Here, θ is regarded as a momentum in a perpendicular synthetic dimension, and σ_m is replaced by $\sigma_{m,\theta}$ in $H_{\text{eff}}(\theta)$. By performing the Fourier transform $\sigma_{m,\theta} = \sum_l e^{-i\theta l}\sigma_{m,l}$, we have $H_{2\text{D}} = -i(\Gamma_0/2)\sum_{mnl} e^{i\varphi|m-n|}\sigma_{m,l}^\dagger\sigma_{n,l} + (V/2)\sum_{ml}(e^{i2k_\Omega dm}\sigma_{m,l}^\dagger\sigma_{m,l+1} + \text{H.c.})$. Similar to conventional quasicrystals [45], the ancestor Hamiltonian $H_{2\text{D}}$ commutes with the magnetic translation group generated by T_m and T_l, where $T_l\sigma_{m,l}T_l^{-1} = \sigma_{m,l+1}$ and $T_m\sigma_{m,l}T_m^{-1} = e^{-i2k_\Omega dm}\sigma_{m+1,l}$. Thus, each gap in the spectrum of $H_{2\text{D}}$ can be characterized by

a quantized and nontrivial Chern number, and this feature is inherited by H_{eff}. As a result, the band topology of H_{eff} can be described by Chern numbers, which satisfies the Diophantine equation $\rho = \mu + \nu(k_\Omega d/\pi)$, where μ is an integer, ν is the Chern number, and ρ is the filling factor within a gap [46–49]. For an irrational $k_\Omega d/\pi$, the Diophantine equation has only one solution when ρ is fixed, thus each gap can be labeled by a set of integers (μ, ν).

Taking Fig. 3(a) as an example, we find that the difference between Chern numbers of neighboring gaps is 1, thus each gap produces a pair of edge states localized on two edges, respectively, according to the bulk-boundary correspondence [50]. This agrees with the number of edge states in Fig. 3(f), and confirms the topological nature of edge states. Furthermore, the modulation phase θ in real arrays can only take discrete values $\theta_n = n\pi - \pi\beta(N+1)$ due to the mirror symmetry inherited from the original Hamiltonian $\mathcal{H}$. As a result, edge states on opposite edges always form degenerate pairs, which is consistent with Fig. 3(a).

Besides edge states, the quasiperiodicity also changes the ergodic nature of subradiant excitations, which is revealed through the analysis of the even-odd (odd-even) energy spacing $S_n^{e-o} = E_{2n} - E_{2n-1}$ ($S_n^{o-e} = E_{2n+1} - E_{2n}$), where E_n are the real eigenenergy parts sorted in ascending order [51,52]. For multifractal states, the spacings exhibit a strongly scattering pattern, while ergodic states possess regular and continuous spacings with open boundary conditions. When η is small, all excitations are ergodic [Fig. 3(g)]. For large η [Fig. 3(h)], bands in the most subradiant regime become multifractal, and the spectrum presents an edge separating the ergodic and multifractal excitations. Such a transition is the result of the interplay between long-ranged hoppings and the effective quasiperiodic potentials. This is confirmed via multifractal analysis on H_{eff} that shows it exhibits a similar multifractal behavior to our system (Appendix C).

The ergodic-multifractal transition is further confirmed by the analysis of fractal dimensions [53–59]. A normalized wave function $|\psi\rangle = \sum_n \psi_n |n\rangle$ can be characterized by the moments $I_q = \sum_n |\psi_n|^{2q} \propto N^{-D_q(q-1)}$, where D_q are fractal dimensions. For ergodic (localized) excitations, $D_q = 1$ ($D_q = 0$), while $D_q \in (0,1)$ for multifractal excitations. In Fig. 3(i), we show the mean fractal dimensions $\bar{D}_2$ over excitations within the same bands. For each band, there exists a critical coupling η at which excitations within this band exhibit multifractal behavior. Thus, subradiant bands become multifractal in sequence when η is increased.

VI. EXPERIMENTAL REALIZATION

For experimental realization, we consider an array of laser-cooled atoms trapped near an optical nanofiber. The atoms are cooled down to their vibrational ground states. Here two-level emitters can be formed by choosing a pair of hyperfine levels, while the harmonic potential can be realized by a state-insensitive optical lattice created by two pairs of counter-propagating beams at the magic wavelengths of the atoms. In this setup, the phonon frequency Ω is around several MHz, while the decay rate Γ_0 is highly tunable and can be adjusted to the same order of magnitude as Ω [60–65]. A typical value of the optomechanical coupling is $\eta \sim 0.05$ for cesium atoms with transition energy $\hbar\omega_0 \sim 1.4\text{eV}$ at $\Omega \sim 1\text{MHz}$. Therefore, the parameter ranges that we consider are accessible in experiments. In the subwavelength limit ($k_0 d \ll 1$), the restriction $\eta \ll k_0 d = \varphi$ should be imposed since the vibrations around the equilibrium positions are assumed to be much smaller than the atomic spacing. Nevertheless, the energy spectrum is already significantly modified in this regime and exhibits visible gaps manifesting the quasiperiodicity. To explore the $\eta \sim \varphi$ regime, a near-Bragg-spaced atomic array with $k_0 d = 2\pi + \varphi$ may be applied.

The nature of the hybrid excitations leads to peculiar dynamical properties that can be exploited as signatures for experimental detection. We consider the emitter array initially prepared in the subradiant state $|k\rangle$ with $k = \pi/d$. In the polariton case, the excitation wave packet is localized in the momentum space with little diffusion. In contrast, hybrid excitations will be scattered into $|k \pm 2nk_\Omega\rangle$ ($n \in \mathbb{Z}$) by phonons, hence the wave packet presents multiple peaks in $k \pm 2nk_\Omega$ after a short of time. For long times, if some of the excitations undergo an ergodic-multifractal transition, the wave packet becomes extended in momentum space but nonergodic. Thus, measuring the momentum distribution $\langle \sigma_k^+ \sigma_k \rangle$ can effectively reveal the characters of the hybrid excitations.

Considering that subradiant excitations are difficult to prepare and detect directly via optical methods, here we propose a scheme for studying hybrid excitations that circumvents these difficulties. Instead of exciting the subradiant state $|\pi/d\rangle$ directly, we can first generate a superradiant excitation $|k_0\rangle$ via a right-propagating coherent-state waveguide probe pulse with frequency resonant to the emitter transition frequency ω_0. The excitation $|k_0\rangle$ can be transferred to $|\pi/d\rangle$ by applying a subsequent momentum shift $U_\phi = \prod_{m=1}^N (|e_m\rangle\langle e_m| + e^{-i\phi z_m}|g_m\rangle\langle g_m|)$ when $\phi = \pi/d - k_0$, which is achieved by geometric phase control [66]. The system is now under free evolution governed by the master equation $\dot{\rho} = -i(H'\rho - \rho H'^{+}) + \sum_{m=1}^N \gamma_m C_m \rho C_m^+$, where $C_m = \sqrt{\gamma_m}|0\rangle\langle\phi_m|$, γ_m and $|\phi_m\rangle$ are eigenvalues and eigenstates of the imaginary part of $-2H'$, respectively.

To obtain the momentum distribution, we finally perform an inversion shift $U_{-\phi-\delta}$ after time T to bring the excitation back to the superradiant regime, allowing it to be detected. δ is a phase offset. The light intensity in the waveguide $I(z,t) = \langle E_R^-(z,t) E_R^+(z,t)\rangle$ is then measured at the right side of the array. Here E_R^+ is the right propagating component of the electric field determined by the emission from emitters into the waveguide, and is given by $E_R^+(z,t) = i\sqrt{N}\Gamma_0 e^{ik_0 z}\sigma_{k_0}(t)/2$ [6]. Thus, the light intensity after performing $U_{-\phi-\delta}$ satisfies

$$I(z, T+0^+) \propto \langle \sigma^+_{\pi/d+\delta}(t-0^+)\sigma_{\pi/d+\delta}(t-0^+)\rangle. \quad (5)$$

By adjusting the offset δ, $\langle \sigma_k^+ \sigma_k \rangle$ can be measured via light intensity I, thus unveils dynamics of excitations. In Fig. 4(a), we simulate the detection scheme and plot the renormalized momentum distribution $P_k = \langle \sigma_k^+ \sigma_k \rangle / C_P$ for polaritons and hybrid excitations, respectively, where $C_P = \sum_k \langle \sigma_k^+ \sigma_k \rangle$. Clearly, these two types of excitations show completely different dynamical properties, which is in agreement with our previous analysis. In Fig. 4(b), we plot $P_{k_0}(T+0^+)$ as a function of offset δ, which is proportional to the light intensity in the waveguide after performing $U_{-\phi-\delta}$. The light intensity

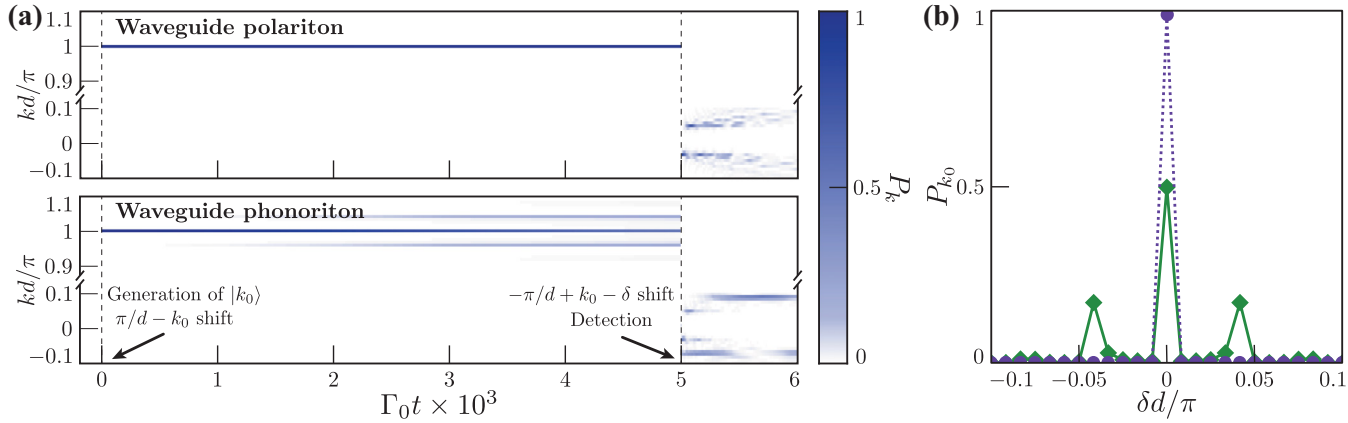

FIG. 4. (a) Renormalized momentum distributions $P_k(t)$ for polaritons (upper panel) and hybrid excitations (lower panel) as a function of time t and momentum k. (b) Renormalized momentum distributions P_{k_0} for polaritons (blue dashed line) and hybrid excitations (green solid line) after the second momentum shift, which is proportional to the light intensity in the waveguide, as a function of δ. The excitation dynamics is obtained by averaging over 5000 quantum trajectories, and has been performed for $10\Gamma_0 = \Omega = 1$, $\varphi = 0.03$, $N = 240$, and $\eta = 0$ ($\eta = 0.06$) in the polariton (hybrid excitations) case.

profile P_{k_0} of hybrid excitations is different from that of polaritons by additional peaks at $\delta = \pm 2nk_\Omega$, and thus successfully captures the dynamical signature of the hybrid excitations.

VII. CONCLUSION

In conclusion, we have shown the emergence of polariton-phonon hybrid excitations with unique properties in a waveguide QED system due to the interplay between waveguide-mediated long-range couplings and phonon scatterings. In a subwavelength finite array, these interactions introduce an effective quasiperiodic structure which leads to the appearance of topological edge states and a transition between ergodic and multifractal excitations. The emergent quasiperiodicity provides an interesting playground for studying one-dimensional quasicrystals due to the infinite-ranged nature of waveguide-mediated couplings, which are vastly different from the tight-binding or long-ranged couplings in typical quasicrystals. Our paper sheds light on the mechanism of interaction between waveguide polaritons and vibrational phonons, and motivates future investigations into exploring many-body physics with waveguide QED systems utilizing emitter vibrations.

ACKNOWLEDGMENTS

This work was supported by National Key R&D Program of China under Grants No. 2021YFA1400900, No. 2021YFA0718300, No. 2021YFA1402100, NSFC under Grants No. 12074027, No. 61835013, No. 12174461, No. 12234012, No. 12334012, No. 52327808, No. 92165207, No. 62225407, Space Application System of China Manned Space Program, the Innovation Program for Quantum Science and Technology under Grant No. 2021ZD0302300, Fundamental Research Funds for the Central Universities, China, under Grant No. FRF-TP-22-098A1, Guangdong Basic and Applied Basic Research Foundation under Grant No. 2023A1515110081, and China Postdoctoral Science Foundation under Grant No. 2020M680725.

APPENDIX A: SCHRIEFFER-WOLFF TRANSFORMATION IN FINITE ARRAYS

In this Appendix, we present a detailed derivation for the SWT performed in finite arrays to decoupled the polaritons from phonons. This is done by finding a proper operator S to cancel the couplings in $e^S H e^{-S}$ to first order, then projecting the transformed Hamiltonian to the single-excitation subspace without phonons [43,44]. The effective Hamiltonian describing polaritons and phonons are given by $H = H_0 + H_p + H_{I1} + H_{I2}$, where

$$\begin{aligned} H_0 &= -i\frac{\Gamma_0}{2}\sum_{m,n} e^{i\varphi|m-n|}\sigma_m^\dagger\sigma_n, \quad H_p = \sum_m \Omega a_m^\dagger a_m, \\ H_{I1} &= \frac{1}{2}\eta\Gamma_0\sum_{m,n}\mathrm{sign}(m-n)e^{ik_0|z_m-z_n|} \\ &\quad\times\sigma_m^\dagger\sigma_n(a_m + a_m^\dagger - a_n - a_n^\dagger), \\ H_{I2} &= -i\frac{1}{4}\eta^2\Gamma\sum_{m,n}^{N} e^{ik_0|z_m-z_n|}\sigma_m^\dagger\sigma_n(a_m + a_m^\dagger - a_n - a_n^\dagger)^2. \end{aligned} \tag{A1}$$

Here we consider the emitter-phonon coupling up to second order in the emitter displacements. The emitter Hamiltonian H_0 can be diagonalized as

$$H_0 = \sum_{\tilde{k}} \varepsilon'_{\tilde{k}}|\psi_{\tilde{k}}\rangle\langle\psi_{\tilde{k}}|, \quad |\psi_{\tilde{k}}\rangle \propto g_{-\tilde{k}}|\widetilde{k}, 0\rangle - g_{\tilde{k}}|-\tilde{k}, 0\rangle, \tag{A2}$$

where $\varepsilon'_{\tilde{k}} = \epsilon_{\tilde{k}} - i\gamma_{\tilde{k}}$ is the eigenvalue of the state $|\psi_{\tilde{k}}\rangle$, and the wave number $\tilde{k}$ satisfies the equation $g_{\tilde{k}}h_{-\tilde{k}} = g_{-\tilde{k}}h_{\tilde{k}}$, $g_{\tilde{k}} = e^{i(\tilde{k}-k_0)z_1}/[1 - e^{i(\tilde{k}-k_0)d}]$ and $h_k = e^{i(k+k_0)z_N}/[e^{-i(k+k_0)d} - 1]$ [29,67]. The operator S should satisfy the condition $[H_0 + H_p, S] = H_{I1}$ to remove the couplings to first order, and is chosen as

$$S = N^{-1/2}\sum_{\tilde{k}_1,\tilde{k}_2,q} |\psi_{\tilde{k}_1}\rangle\langle\psi_{\tilde{k}_2}|\left(A_{\tilde{k}_1,\tilde{k}_2,q}a_q + B_{\tilde{k}_1,\tilde{k}_2,q}a_{-q}^\dagger\right). \tag{A3}$$

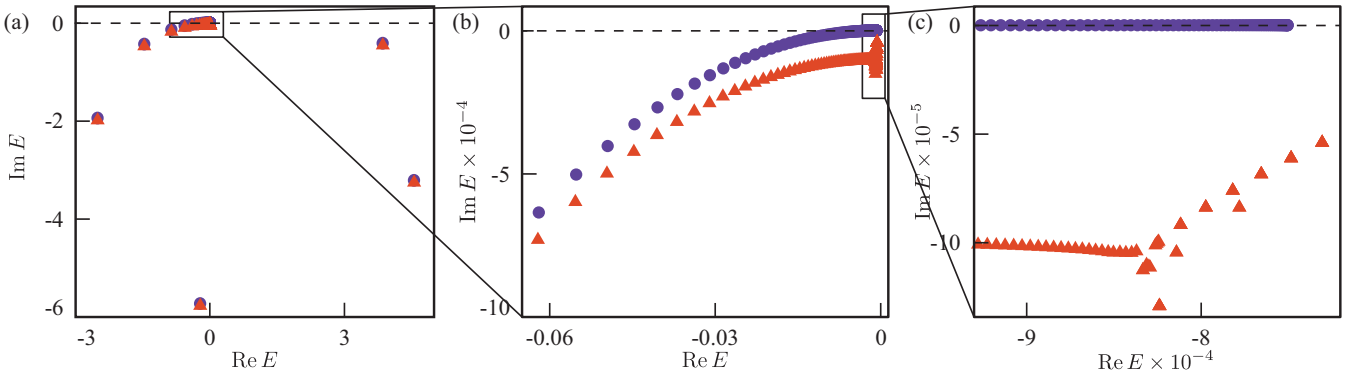

FIG. 5. Complex single-excitation spectrums obtained from the Schrieffer-Wolff transformation results Eq. (A5) (red triangle) in comparison with the single-polariton spectrums (blue circle). The spectrums are zoomed in different scales. Here the system parameters are selected to be the same as Fig. 2(a) in the main text: $10\Gamma_0 = \Omega = 1$, $\varphi = 0.03$, $\eta/\varphi = 1$, and $N = 240$.

The couplings H_{I1} can be written as $H_{I1} = N^{-1/2}\sum_{\tilde{k}_1,\tilde{k}_2,q}\tilde{g}_{\tilde{k}_1,\tilde{k}_2,q}|\psi_{\tilde{k}_1}\rangle\langle\psi_{\tilde{k}_2}|(a_q + a^\dagger_{-q})$, thus the coefficients A and B can be obtained as

$$A_{\tilde{k}_1,\tilde{k}_2,q} = \frac{\tilde{g}_{\tilde{k}_1,\tilde{k}_2,q}}{-\Omega + \varepsilon'_{\tilde{k}_1} - \varepsilon'_{\tilde{k}_2}}, \quad B_{\tilde{k}_1,\tilde{k}_2,q} = \frac{\tilde{g}_{\tilde{k}_1,\tilde{k}_2,q}}{\Omega + \varepsilon'_{\tilde{k}_1} - \varepsilon'_{\tilde{k}_2}}. \tag{A4}$$

Therefore, the effective Hamiltonian to the second order of η is given by

$$\begin{aligned} H' &= H_0 + \frac{1}{2}P_0([S, H_{I1}] + H_{I2})P_0 \\ &= (1-\eta^2)H_0 - i\frac{1}{2}\eta^2\Gamma_0 + \sum_{\tilde{k}_1,\tilde{k}_2}\Delta_{\tilde{k}_1,\tilde{k}_2}|\psi_{\tilde{k}_1}\rangle\langle\psi_{\tilde{k}_2}|, \quad \Delta_{\tilde{k}_1,\tilde{k}_2} \\ &= \frac{1}{2N}\sum_{q,\tilde{k}}\tilde{g}_{\tilde{k},\tilde{k}_2,-q}\left(A_{\tilde{k}_1,\tilde{k},q} - B_{\tilde{k}_1,\tilde{k},q}\right), \end{aligned} \tag{A5}$$

where P_0 is the projector onto the subspace with zero phonons. The excitation spectrum can be obtained by diagonalizing H', as shown in Figs. 5 and 6. It is clear that the spectrum is modified significantly in the most subradiant regime compared to the polariton spectrum.

To complete the derivation, we need to ensure the validity of the SWT. To perform the SWT correctly, the single-polariton subspace without phonons should be separated from the rest of the spectrum by an energy gap, such that the strength of the interaction Hamiltonian H_{I1} is much smaller than the energy gap [43,44]. This condition can be written as

$$|\langle\psi_{\tilde{k}'}, q|H_{I1}|\psi_{\tilde{k}}\rangle| \ll |\varepsilon'_{\tilde{k}',q} - \varepsilon'_{\tilde{k}}|, \tag{A6}$$

where $\varepsilon'_{\tilde{k}}$ and $\varepsilon'_{\tilde{k}',q} = \varepsilon'_{\tilde{k}'} + \Omega$ are the eigenvalues of the states $|\psi_{\tilde{k}}\rangle$ and $|\psi_{\tilde{k}'}, q\rangle = a^\dagger_q|\psi_{\tilde{k}'}\rangle$, respectively.

To proceed, we note that the eigenvalue $\varepsilon'_{\tilde{k}}$ can be approximated by

$$\varepsilon'_{\tilde{k}} = \epsilon_{\tilde{k}} - i\gamma_{\tilde{k}} \approx \varepsilon_k - i\gamma_{\tilde{k}}, \tag{A7}$$

where

$$\varepsilon_k = \frac{\Gamma_0}{4}f(k) - i\frac{N\Gamma_0}{4}\delta_{k,\pm k_0}, \tag{A8}$$

is the eigenvalue of H_0 in an infinite array, $f(k) = \cot(k_0 d/2 - kd/2) + \cot(k_0 d/2 + kd/2)$, and $k = \mathrm{Re}\,\tilde{k}$. Meanwhile, the matrix element of H_{I1} can be estimated by

$$|\langle\psi_{\tilde{k}'}, q|H_{I1}|\psi_{\tilde{k}}\rangle| \sim |\langle k', q|H_{I1}|k, 0\rangle| \approx N^{-1/2}g_{k,-q}\delta_{k',k-q}, \tag{A9}$$

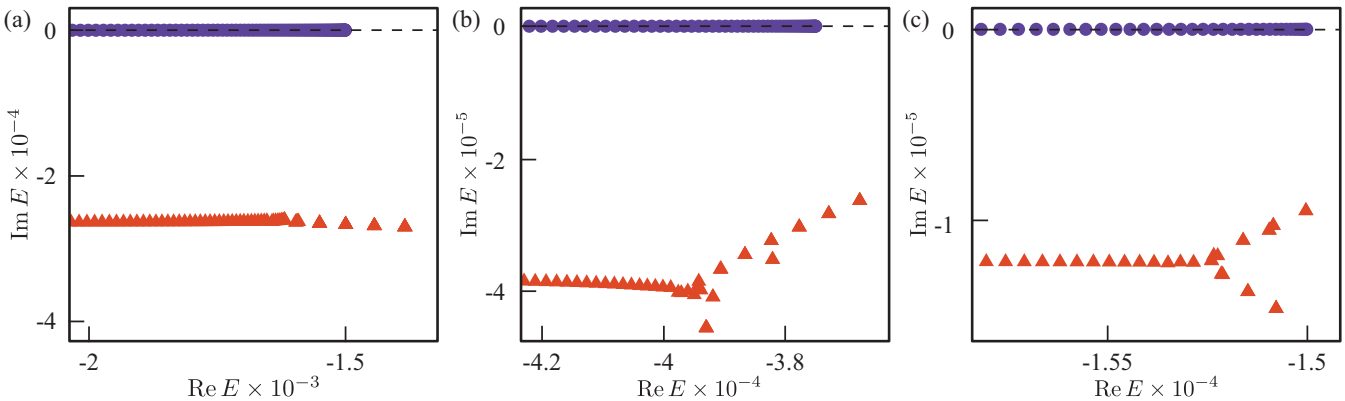

FIG. 6. The most subradiant part of the complex single-excitation spectrum obtained from the Schrieffer-Wolff transformation results Eq. (A5) (red triangle) in comparison with the single-polariton spectrums (blue circle). The calculation has been performed for $\Omega = 1$, $\eta/\varphi = 1$, $N = 240$, and $\Gamma_0 = 0.1$, $\varphi = 0.06$ in (a), $\Gamma_0 = 0.05$, $\varphi = 0.03$ in (b), and $\Gamma_0 = 0.02$, $\varphi = 0.03$ in (c), respectively.

since H_{I1} perturbs the single-polariton state $|k,0\rangle = \sigma_k^\dagger|0\rangle$ and only connects it to $|k-q,q\rangle = \sigma_{k-q}^\dagger a_q^\dagger|0\rangle$ in an infinite array.

In infinite arrays, the condition Eq. (A6) fails near $q = k \pm k_\Omega$, where $k_\Omega > 0$ is determined by $\varepsilon_k = \Omega + \varepsilon_{k_\Omega}$, since the single-polariton state $|k,0\rangle$ is degenerated with $|\pm k_\Omega, k \mp k_\Omega\rangle$. However, this degeneracy is lifted in finite arrays due to the discrepancy in their decay rates. There exists an imaginary energy gap $\Delta \approx i(\gamma_{\tilde{k}_\Omega} - \gamma_{\tilde{k}})$ separating states $|\psi_{\tilde{k}}\rangle$ and $|\psi_{\pm\tilde{k}_\Omega}, k \mp k_\Omega\rangle$. Therefore, the condition Eq. (A6) can be satisfied if this energy gap is much larger than the corresponding matrix element of H_{I1}. This is equivalent to

$$|\gamma_{\tilde{k}_\Omega} - \gamma_{\tilde{k}}| \gg |\langle \pm k_\Omega, k \mp k_\Omega | H_{I1} | k, 0\rangle|. \tag{A10}$$

For subradiant excitation $k \approx \pi/d$, its decay rate scales as [29]

$$\gamma_{\tilde{k}} \sim N^{-1}\Gamma_0\varphi^2(k - \pi/d)^2. \tag{A11}$$

Meanwhile, the decay rate $\gamma_{\tilde{k}_\Omega}$ can be calculated as follows. Supposing $\tilde{k}_\Omega = k_\Omega + \delta/N$, then δ describes the correction to the wave number. According to the equation $g_{\tilde{k}_\Omega} h_{-\tilde{k}_\Omega} = g_{-\tilde{k}_\Omega} h_{\tilde{k}_\Omega}$, we can find that $\delta \approx -i\varphi/(k_\Omega d)$ when $\varphi \ll k_\Omega d \ll 1$. Next, we substitute $\tilde{k}_\Omega$ into the expression for ε_k (Eq. (A8)), then this imaginary correction leads to the decay rate:

$$\gamma_{\tilde{k}_\Omega} \sim N^{-1}\Omega^2\Gamma_0^{-1}. \tag{A12}$$

It is clear that $\gamma_{\tilde{k}_\Omega} \gg \gamma_{\tilde{k}}$, thus the spectral gap Δ scales as $\Delta \approx i\gamma_{\tilde{k}_\Omega} \sim iN^{-1}\Omega^2\Gamma_0^{-1}$. Meanwhile, we have

$$\begin{aligned} |\langle \pm k_\Omega, k \mp k_\Omega | H_{I1} | k, 0\rangle| &= N^{-1/2} g_{k,\pm k_\Omega - k} \\ &\approx N^{-1/2}\eta\Gamma_0(\varphi\Gamma_0/\Omega)^{-1/2}, \end{aligned} \tag{A13}$$

in the same regime $\varphi \ll k_\Omega d \ll 1$. Therefore, the condition Eq. (A6) is equivalent to

$$\eta^2\varphi^{-1}(\Gamma_0/\Omega)^3 \ll N^{-1}. \tag{A14}$$

Hence, the SWT is well-defined and provides correct results in the weak coupling regime $\eta \ll 1$ if $\eta\varphi^{-1}(\Gamma_0/\Omega)^3$ scales as $N^{-s}(s \geqslant 1)$. This is achievable in experiments since both the decay rate Γ_0 and the atomic spacing d are highly tunable. For example, we can maintain $\Gamma_0/\Omega \sim N^{-1/3}$ while η and φ remain unchanged as the system size N increases. In all figures of the main text, the parameters are chosen such that the condition Eq. (A14) is fulfilled. This justifies the validity of the SWT in our paper.

APPENDIX B: THE EMERGENCE OF QUASIPERIODIC STRUCTURE

In this Appendix, we focus on the effects of resonant phonon processes on the phonon correction $\Delta = \sum \Delta_{\tilde{k}_1,\tilde{k}_2} |\psi_{\tilde{k}_1}\rangle\langle\psi_{\tilde{k}_2}|$ and present a derivation for the approximate effective Hamiltonian H_{eff} in the main text. We first replace the discrete sum $\sum_{\tilde{k}}$ in Eq. (A5) by the integral $(2\pi)^{-1}\int d\tilde{k}$. In the expression

$$\frac{1}{-\Omega + \varepsilon'_{\tilde{k}_1} - \varepsilon'_{\tilde{k}_2}} = \frac{1}{-\Omega + \epsilon_{\tilde{k}_1} - \epsilon_{\tilde{k}_2} + i\left(\gamma_{\tilde{k}_2} - \gamma_{\tilde{k}_1}\right)}, \tag{B1}$$

the decay rates $\gamma_{\tilde{k}_1}$ and $\gamma_{\tilde{k}_2}$ are much smaller than other energy scales and satisfy $\gamma_{\tilde{k}_2} > \gamma_{\tilde{k}_1}$ for subradiant states on the lower branch of the spectrum with $-\Omega + \epsilon_{\tilde{k}_1} - \epsilon_{\tilde{k}_2} = 0$. Therefore, we can replace $i(\gamma_{\tilde{k}_2} - \gamma_{\tilde{k}_1})$ by $i0^+$ and apply the Sokhotski formula:

$$\frac{1}{-\Omega + \varepsilon'_{\tilde{k}_1} - \varepsilon'_{\tilde{k}_2}} \approx \mathcal{P}\frac{1}{-\Omega + \epsilon_{\tilde{k}_1} - \epsilon_{\tilde{k}_2}} - i\pi\delta\left(-\Omega + \epsilon_{\tilde{k}_1} - \epsilon_{\tilde{k}_2}\right). \tag{B2}$$

Thus, we can separate the phonon correction as $\Delta = \Delta' + \Delta''$, where

$$\Delta'_{\tilde{k}_1,\tilde{k}_2} = \frac{1}{4\pi}\sum_q \mathcal{P}\int d\tilde{k}\,\tilde{g}_{\tilde{k},\tilde{k}_2,-q}\left(A_{\tilde{k}_1,\tilde{k},q} - B_{\tilde{k}_1,\tilde{k},q}\right) \tag{B3}$$

describes the energy shift to the excitation, and

$$\begin{aligned} \Delta''_{\tilde{k}_1,\tilde{k}_2} = &-\frac{i}{4}\sum_q \int d\tilde{k}\,\tilde{g}_{\tilde{k},\tilde{k}_2,-q}\tilde{g}_{\tilde{k}_1,\tilde{k},q} \\ &\times\left(\delta\left(-\Omega + \epsilon_{\tilde{k}_1} - \epsilon_{\tilde{k}}\right) + \delta\left(-\Omega + \epsilon_{\tilde{k}_2} - \epsilon_{\tilde{k}}\right)\right). \end{aligned} \tag{B4}$$

Similar to the previous discussions, the solution of $-\Omega + \epsilon_{\tilde{k}_{1(2)}} - \epsilon_{\tilde{k}} = 0$ can be approximately given by $\tilde{k} = k_\Omega$ if we consider phonon corrections to the states in the quasiflat regime. In the k space, the corrections Δ'' can be evaluated as

$$\begin{aligned} \Delta''_{k_1,k_2} &= \sum_{\tilde{k}_1,\tilde{k}_2} \Delta''_{\tilde{k}_1,\tilde{k}_2}\langle k_1|\psi_{\tilde{k}_1}\rangle\langle\psi_{\tilde{k}_2}|k_2\rangle \\ &= -\frac{i}{2|\varepsilon'_{k_\Omega}|}\sum_{\tilde{k}_1,\tilde{k}_2,q} \tilde{g}_{k_\Omega,\tilde{k}_2,-q}\tilde{g}_{\tilde{k}_1,k_\Omega,q}\langle k_1|\psi_{\tilde{k}_1}\rangle\langle\psi_{\tilde{k}_2}|k_2\rangle \\ &= -\frac{i}{2|\varepsilon'_{k_\Omega}|}\sum_q g_{k_2,-q}g_{k_1-q,q}\langle\psi_{k_\Omega}|k_2 - q\rangle\langle k_1 - q|\psi_{k_\Omega}\rangle. \end{aligned} \tag{B5}$$

The eigenstate $|\psi_{k_\Omega}\rangle$ can be approximated by $|\psi_{k_\Omega}\rangle \approx (|k_\Omega\rangle + |-k_\Omega\rangle)/\sqrt{2}$ since $g_{\tilde{k}} \approx -g_{-\tilde{k}}$ when $\varphi \ll k_\Omega \ll 1$. Thus,

$$\Delta''_{k_1,k_2} = -\frac{i}{8}\eta^2\Gamma_0\left(\frac{\Gamma_0}{\Omega\varphi}\right)^{\frac{1}{2}}(2\delta_{k_1,k_2} + \delta_{k_1,k_2+2k_\Omega} + \delta_{k_1,k_2-2k_\Omega}), \tag{B6}$$

where we use the facts that $g_{k_\Omega - q,q} \approx -g_{k_{\Omega,q}} = i\eta\Gamma_0 f(k_\Omega)/4$. Thus, we have

$$\begin{aligned} \Delta'' = &-\frac{i}{8}\eta^2\Gamma_0\left(\frac{\Gamma_0}{\Omega\varphi}\right)^{\frac{1}{2}}\sum_k (2|k\rangle\langle k| \\ &+ |k\rangle\langle k + 2k_\Omega| + |k + 2k_\Omega\rangle\langle k|). \end{aligned} \tag{B7}$$

For a finite array, the Sokhotski formula cannot exactly describe the behavior of $(-\Omega + \varepsilon'_{\tilde{k}_1} - \varepsilon'_{\tilde{k}_2})^{-1}$ due to the discreteness of energy spectrum. This leads to the deviations from Eq. (B7) and requires the introductions of k-dependent coefficients. As a result, the phonon correction Δ has the form

$$\begin{aligned} \Delta \approx &\sum_k [V_k(e^{-i\theta_k}|k\rangle\langle k + 2k_\Omega| + e^{i\theta_k}|k + 2k_\Omega\rangle\langle k|)/2 \\ &+ \delta\varepsilon_k|k\rangle\langle k|], \end{aligned} \tag{B8}$$

where V_k and θ_k are the k-dependent coupling strength and phase factor respectively, and $\delta\varepsilon_k$ is the energy shift.

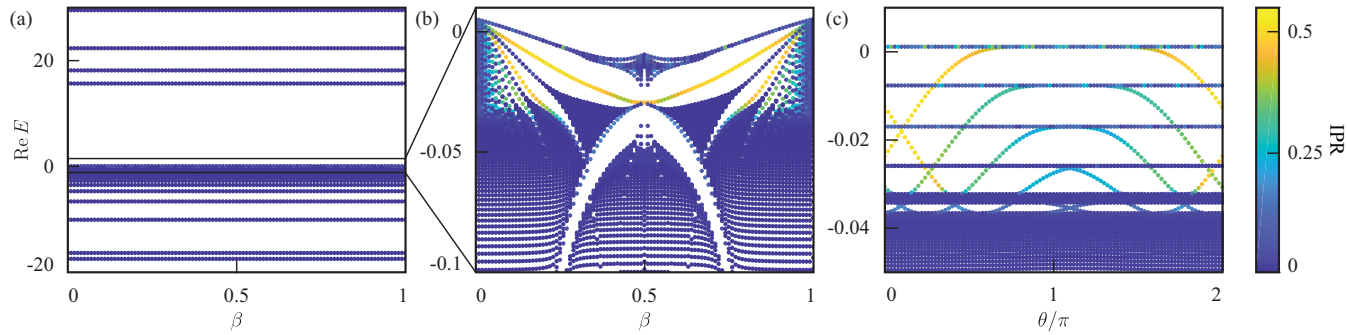

FIG. 7. (a), (b) Real spectrum of H_{eff} [Eq. (B9)] zoomed in different scales as a function of β with $\theta = 0$. (c) Real spectrum of the most subradiant excitations in H_{eff} as a function of θ with $\beta = 1/(10+\beta) = \sqrt{26} - 5$. All these were generated for an array of $N = 200$ emitters with $\Gamma_0 = 1$, $\varphi = 0.059$, and $V = 0.02$.

Coefficients V_k, θ_k, and $\delta\varepsilon_k$ change slowly in the subradiant regime, thus we can replace them by their values at $k = \pi/d$ if we are only concerned about subradiant excitations. Omitting the energy shift $\delta\varepsilon = \delta\varepsilon_{k=\pi/d}$, the resulting effective Hamiltonian in real space can be written as

$$H' \approx H_{\text{eff}} = H_0 + V\sum_m \cos(2\pi\beta m + \theta)|m\rangle\langle m|, \qquad \text{(B9)}$$

where $V = V_{k=\pi/d}$, $\theta = \theta_{k=\pi/d}$, and $\beta = k_\Omega d/\pi$ serves as the frequency.

H_{eff} can be regarded as a one-dimensional quasiperiodic model since β is determined by the transcendental equation $\varepsilon_k = \Omega + \varepsilon_{k_\Omega}$ and is, in general, irrational. Due to the quasiperiodicity, the spectrum of H_{eff} becomes very rich and exhibits a characteristic Hofstadter butterfly pattern, as shown in Fig. 7(b). Furthermore, the spectrum also includes highly localized edge states which cross the spectral gaps by changing the modulation phase θ [Fig. 7(c)]. These properties clearly hint at the topological nature of the spectral gaps and edge states.

APPENDIX C: MULTIFRACTALITY IN THE EFFECTIVE HAMILTONIAN H_{eff}

In this Appendix, we perform a multifractal analysis on the effective Hamiltonian H_{eff} and reveal that it presents a similar ergodic-multifractal transition to the system we considered. The effective Hamiltonian H_{eff} reads

$$H_{\text{eff}} = -i\frac{\Gamma_0}{2}\sum_{m,n} e^{i\varphi|m-n|}|m\rangle\langle n| + V\sum_m \cos(2\pi\beta m + \theta)|m\rangle\langle m|, \qquad \text{(C1)}$$

where β is the modulation frequency.

Similar to the main text, we employ the fractal dimensions and the level spacings to distinguish ergodic and multifractal regions of the spectrum. We first compute the even-odd (odd-even) energy spacing $S_n^{e-o} = E_{2n} - E_{2n-1}$ ($S_n^{o-e} = E_{2n+1} - E_{2n}$) in Figs. 8(a) and 8(b), where E_n are the real parts of eigenenergies sorted in ascending order. It is clear that all states are ergodic when the potential strength V is small. For larger V, we can find that several bands become multifractal and exhibit strongly scattered distributions. An ergodic-to-multifractal edge separating two regions can also be identified.

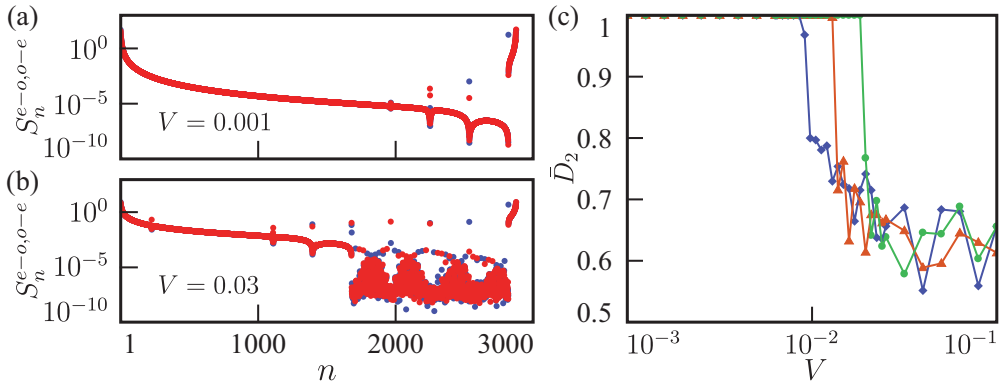

FIG. 8. (a), (b) Level spacing S_n^{e-o} (red) and S_n^{o-e} (blue) for the effective Hamiltonian H_{eff} [Eq. (C1)] with $V = 0.001$ (a) and $V = 0.03$ (b), respectively. (c). Mean fractal dimensions $\bar{D}_2$ for three subbands with highest energy. Three subbands (blue diamond, red triangle, green circle) are arranged in energy-descending order. All these were generated for an array of $N = 5760$ emitters with $\Gamma_0 = \Omega = 1$, $\varphi = \pi/50$, $\beta = 1/(10+\beta) = \sqrt{26} - 5$, and $\theta = 0$.

To determine the fractal dimension, we follow the standard box-counting procedure by dividing the system into N/l boxes of size l [53,55,56]. For a normalized wave function $|\psi\rangle = \sum_n \psi_n |n\rangle$, the probability in the ith box is given by $\mu_i = \sum_n |\psi_n|^2$, where the summation is performed inside the ith box. The spectrum of fractal dimensions is given by

$$f(\alpha_q) = \lim_{\delta\to 0} \frac{\sum_{i=1}^{N/l} \mu_i(q) \ln \mu_i(q)}{\ln \delta},$$

$$\alpha_q = \lim_{\delta\to 0} \frac{\sum_{i=1}^{N/l} \mu_i(q) \ln \mu_i(1)}{\ln \delta}, \tag{C2}$$

where $\delta = l/N$, $\mu_i(q) = \mu_i^q / \sum_{i=1}^{N/l} \mu_i^q$ is the normalized qth moment. Meanwhile, $|\psi\rangle$ can be characterized by the moment $I_q = \sum_n |\psi_n|^{2q} \propto N^{-\tau(q)}$, where $\tau(q)$ is related to $f(\alpha_q)$ via the Legendre transform $\tau(q) = q\alpha_q - f(\alpha_q)$. The fractal dimension D_q is given by $D_q = \tau(q)/(q-1)$. In Fig. 8(c), we show the mean fractal dimensions $\bar{D}_2$ for three bands with highest energy. It can be found that the ergodic-multifractal transitions happened at different potential strengths V for each band, and bands with lower energies require larger V to become multifractal. These analyses confirm the presence of ergodic-multifractal transitions in the effective Hamiltonian H_{eff}.

[1] P. Forn-Diaz, J. J. Garcia-Ripoll, B. Peropadre, J. L. Orgiazzi, M. A. Yurtalan, R. Belyansky, C. M. Wilson, and A. Lupascu, Ultrastrong coupling of a single artificial atom to an electromagnetic continuum in the nonperturbative regime, Nat. Phys. **13**, 39 (2017).

[2] M. Mirhosseini, E. Kim, X. Zhang, A. Sipahigil, P. B. Dieterle, A. J. Keller, A. Asenjo-Garcia, D. E. Chang, and O. Painter, Cavity quantum electrodynamics with atom-like mirrors, Nature (London) **569**, 692 (2019).

[3] B. Kannan, M. J. Ruckriegel, D. L. Campbell, A. Frisk Kockum, J. Braumuller, D. K. Kim, M. Kjaergaard, P. Krantz, A. Melville, B. M. Niedzielski, A. Vepsalainen, R. Winik, J. L. Yoder, F. Nori, T. P. Orlando, S. Gustavsson, and W. D. Oliver, Waveguide quantum electrodynamics with superconducting artificial giant atoms, Nature (London) **583**, 775 (2020).

[4] M. Zanner, T. Orell, C. M. F. Schneider, R. Albert, S. Oleschko, M. L. Juan, M. Silveri, and G. Kirchmair, Coherent control of a multi-qubit dark state in waveguide quantum electrodynamics, Nat. Phys. **18**, 538 (2022).

[5] B. Kannan, A. Almanakly, Y. Sung, A. Di Paolo, D. A. A. Rower, J. Braumueller, A. Melville, B. M. M. Niedzielski, A. Karamlou, K. Serniak, A. Vepsaelaeinen, M. E. E. Schwartz, J. L. L. Yoder, R. Winik, J. I.-J. Wang, T. P. P. Orlando, S. Gustavsson, J. A. A. Grover, and W. D. D. Oliver, On-demand directional microwave photon emission using waveguide quantum electrodynamics, Nat. Phys. **19**, 394 (2023).

[6] A. Asenjo-Garcia, M. Moreno-Cardoner, A. Albrecht, H. J. Kimble, and D. E. Chang, Exponential improvement in photon storage fidelities using subradiance and "selective radiance" in atomic arrays, Phys. Rev. X **7**, 031024 (2017).

[7] A. Albrecht, L. Henriet, A. Asenjo-Garcia, P. B. Dieterle, O. Painter, and D. E. Chang, Subradiant states of quantum bits coupled to a one-dimensional waveguide, New J. Phys. **21**, 025003 (2019).

[8] Y. Marques, I. A. Shelykh, and I. V. Iorsh, Two-dimensional chiral-waveguide quantum electrodynamics: Long-range qubit correlations and flat-band dark polaritons, Phys. Rev. A **103**, 033702 (2021).

[9] Z. Li, S. Choudhury, and W. V. Liu, Long-range-ordered phase in a quantum Heisenberg chain with interactions beyond nearest neighbors, Phys. Rev. A **104**, 013303 (2021).

[10] E. Kim, X. Zhang, V. S. Ferreira, J. Banker, J. K. Iverson, A. Sipahigil, M. Bello, A. González-Tudela, M. Mirhosseini, and O. Painter, Quantum electrodynamics in a topological waveguide, Phys. Rev. X **11**, 011015 (2021).

[11] J. Perczel, J. Borregaard, D. E. Chang, S. F. Yelin, and M. D. Lukin, Topological quantum optics using atomlike emitter arrays coupled to photonic crystals, Phys. Rev. Lett. **124**, 083603 (2020).

[12] M. Bello, G. Platero, J. I. Cirac, and A. González-Tudela, Unconventional quantum optics in topological waveguide qed, Sci. Adv. **5**, eaaw0297 (2019).

[13] T. L. Patti, D. S. Wild, E. Shahmoon, M. D. Lukin, and S. F. Yelin, Controlling interactions between quantum emitters using atom arrays, Phys. Rev. Lett. **126**, 223602 (2021).

[14] M. Moreno-Cardoner, D. Goncalves, and D. E. Chang, Quantum nonlinear optics based on two-dimensional Rydberg atom arrays, Phys. Rev. Lett. **127**, 263602 (2021).

[15] G. Ferioli, A. Glicenstein, L. Henriet, I. Ferrier-Barbut, and A. Browaeys, Storage and release of subradiant excitations in a dense atomic cloud, Phys. Rev. X **11**, 021031 (2021).

[16] D. Fernández-Fernández and A. González-Tudela, Tunable directional emission and collective dissipation with quantum metasurfaces, Phys. Rev. Lett. **128**, 113601 (2022).

[17] Y.-X. Zhang and K. Mølmer, Free-fermion multiply excited eigenstates and their experimental signatures in 1D arrays of two-level atoms, Phys. Rev. Lett. **128**, 093602 (2022).

[18] R. Holzinger, R. Gutiérrez-Jáuregui, T. Hönigl-Decrinis, G. Kirchmair, A. Asenjo-Garcia, and H. Ritsch, Control of localized single- and many-body dark states in waveguide QED, Phys. Rev. Lett. **129**, 253601 (2022).

[19] A. S. Prasad, J. Hinney, S. Mahmoodian, K. Hammerer, S. Rind, P. Schneeweiss, A. S. Sørensen, J. Volz, and A. Rauschenbeutel, Correlating photons using the collective nonlinear response of atoms weakly coupled to an optical mode, Nat. Photon. **14**, 719 (2020).

[20] B. Kannan, D. L. Campbell, F. Vasconcelos, R. Winik, D. K. Kim, M. Kjaergaard, P. Krantz, A. Melville, B. M. Niedzielski, J. L. Yoder, T. P. Orlando, S. Gustavsson, and W. D. Oliver, Generating spatially entangled itinerant photons with waveguide quantum electrodynamics, Sci. Adv. **6**, eabb8780 (2020).

[21] O. A. Iversen and T. Pohl, Strongly correlated states of light and repulsive photons in chiral chains of three-level quantum emitters, Phys. Rev. Lett. **126**, 083605 (2021).

[22] Y. Marques, I. A. Shelykh, and I. V. Iorsh, Bound photonic pairs in 2D waveguide quantum electrodynamics, Phys. Rev. Lett. **127**, 273602 (2021).

[23] D. E. Chang, J. I. Cirac, and H. J. Kimble, Self-organization of atoms along a nanophotonic waveguide, Phys. Rev. Lett. **110**, 113606 (2013).

[24] E. Sánchez-Burillo, A. González-Tudela, and C. Gonzalez-Ballestero, Theory of waveguide QED with moving emitters, Phys. Rev. A **102**, 013726 (2020).

[25] J. Anglin and W. Ketterle, Bose-Einstein condensation of atomic gases, Nature (London) **416**, 211 (2002).

[26] I. Iorsh, A. Poshakinskiy, and A. Poddubny, Waveguide quantum optomechanics: Parity-time phase transitions in ultrastrong coupling regime, Phys. Rev. Lett. **125**, 183601 (2020).

[27] D. D. Sedov, V. K. Kozin, and I. V. Iorsh, Chiral waveguide optomechanics: First order quantum phase transitions with $\mathbb{Z}_3$ symmetry breaking, Phys. Rev. Lett. **125**, 263606 (2020).

[28] A. Poshakinskiy, I. Iorsh, and A. Poddubny, Localized multiphonon states in waveguide quantum optomechanics with spontaneously broken $\mathcal{PT}$ symmetry, Phys. Rev. A **104**, 063719 (2021).

[29] Y.-X. Zhang and K. Mølmer, Theory of subradiant states of a one-dimensional two-level atom chain, Phys. Rev. Lett. **122**, 203605 (2019).

[30] J. Zhong, N. A. Olekhno, Y. Ke, A. V. Poshakinskiy, C. Lee, Y. S. Kivshar, and A. N. Poddubny, Photon-mediated localization in two-level qubit arrays, Phys. Rev. Lett. **124**, 093604 (2020).

[31] A. V. Poshakinskiy, J. Zhong, Y. Ke, N. A. Olekhno, C. Lee, Y. S. Kivshar, and A. N. Poddubny, Quantum Hall phases emerging from atom–photon interactions, NPJ Quantum Inf. **7**, 34 (2021).

[32] Y.-X. Zhang, C. Yu, and K. Mølmer, Subradiant bound dimer excited states of emitter chains coupled to a one dimensional waveguide, Phys. Rev. Res. **2**, 013173 (2020).

[33] A. V. Poshakinskiy and A. N. Poddubny, Dimerization of many-body subradiant states in waveguide quantum electrodynamics, Phys. Rev. Lett. **127**, 173601 (2021).

[34] A. V. Poshakinskiy, J. Zhong, and A. N. Poddubny, Quantum chaos driven by long-range waveguide-mediated interactions, Phys. Rev. Lett. **126**, 203602 (2021).

[35] S. Mahmoodian, G. Calajo, D. E. Chang, K. Hammerer, and A. S. Sorensen, Dynamics of many-body photon bound states in chiral waveguide qed, Phys. Rev. X **10**, 031011 (2020).

[36] J. Zhong and A. N. Poddubny, Classification of three-photon states in waveguide quantum electrodynamics, Phys. Rev. A **103**, 023720 (2021).

[37] A. S. Sheremet, M. I. Petrov, I. V. Iorsh, A. V. Poshakinskiy, and A. N. Poddubny, Waveguide quantum electrodynamics: Collective radiance and photon-photon correlations, Rev. Mod. Phys. **95**, 015002 (2023).

[38] T. Shi, S. Fan, and C. P. Sun, Two-photon transport in a waveguide coupled to a cavity in a two-level system, Phys. Rev. A **84**, 063803 (2011).

[39] J. I. Cirac, A. S. Parkins, R. Blatt, and P. Zoller, "Dark" squeezed states of the motion of a trapped ion, Phys. Rev. Lett. **70**, 556 (1993).

[40] J. S. Pedernales, I. Lizuain, S. Felicetti, G. Romero, L. Lamata, and E. Solano, Quantum Rabi model with trapped ions, Sci. Rep. **5**, 15472 (2015).

[41] R. Puebla, M.-J. Hwang, J. Casanova, and M. B. Plenio, Probing the dynamics of a superradiant quantum phase transition with a single trapped ion, Phys. Rev. Lett. **118**, 073001 (2017).

[42] H.-J. Zhu, K. Xu, G.-F. Zhang, and W.-M. Liu, Finite-component multicriticality at the superradiant quantum phase transition, Phys. Rev. Lett. **125**, 050402 (2020).

[43] S. Bravyi, D. P. DiVincenzo, and D. Loss, Schrieffer-Wolff transformation for quantum many-body systems, Ann. Phys. **326**, 2793 (2011).

[44] P. Coleman, *Introduction to Many-Body Physics* (Cambridge University Press, Cambridge, 2015).

[45] Y. E. Kraus and O. Zilberberg, Topological equivalence between the Fibonacci quasicrystal and the Harper model, Phys. Rev. Lett. **109**, 116404 (2012).

[46] B. X. Wang and C. Y. Zhao, Topological quantum optical states in quasiperiodic cold atomic chains, Phys. Rev. A **103**, 013727 (2021).

[47] O. Zilberberg, Topology in quasicrystals, Opt. Mater. Express **11**, 1143 (2021).

[48] Y. Ren, Z. Qiao, and Q. Niu, Topological phases in two-dimensional materials: A review, Rep. Prog. Phys. **79**, 066501 (2016).

[49] Q. Niu, Advances on topological materials, Front. Phys. **15**, 43601 (2020).

[50] Y. E. Kraus, Y. Lahini, Z. Ringel, M. Verbin, and O. Zilberberg, Topological states and adiabatic pumping in quasicrystals, Phys. Rev. Lett. **109**, 106402 (2012).

[51] X. Deng, S. Ray, S. Sinha, G. V. Shlyapnikov, and L. Santos, One-dimensional quasicrystals with power-law hopping, Phys. Rev. Lett. **123**, 025301 (2019).

[52] M. Sarkar, R. Ghosh, A. Sen, and K. Sengupta, Mobility edge and multifractality in a periodically driven Aubry-André model, Phys. Rev. B **103**, 184309 (2021).

[53] E. Cuevas, $f(\alpha)$ multifractal spectrum at strong and weak disorder, Phys. Rev. B **68**, 024206 (2003).

[54] J. Biddle and S. Das Sarma, Predicted mobility edges in one-dimensional incommensurate optical lattices: An exactly solvable model of Anderson localization, Phys. Rev. Lett. **104**, 070601 (2010).

[55] A. Jagannathan, The fibonacci quasicrystal: Case study of hidden dimensions and multifractality, Rev. Mod. Phys. **93**, 045001 (2021).

[56] Z. Xu, X. Xia, and S. Chen, Non-hermitian Aubry-André model with power-law hopping, Phys. Rev. B **104**, 224204 (2021).

[57] B. Huang and W. V. Liu, Moiré localization in two-dimensional quasiperiodic systems, Phys. Rev. B **100**, 144202 (2019).

[58] P. Wang, Y. Zheng, X. Chen, C. Huang, Y. V. Kartashov, L. Torner, V. V. Konotop, and F. Ye, Localization and delocalization of light in photonic moire lattices, Nature (London) **577**, 42 (2020).

[59] D. A. Zezyulin and V. V. Konotop, Localization of ultracold atoms in zeeman lattices with incommensurate spin-orbit coupling, Phys. Rev. A **105**, 063323 (2022).

[60] R. Gerritsma, G. Kirchmair, F. Zähringer, E. Solano, R. Blatt, and C. F. Roos, Quantum simulation of the Dirac equation, Nature (London) **463**, 68 (2010).

[61] P. Solano, Y. Duan, Y.-T. Chen, A. Rudelis, C. Chin, and V. Vuletic, Strongly correlated quantum gas prepared by direct laser cooling, Phys. Rev. Lett. **123**, 173401 (2019).

[62] B. J. DeSalvo, K. Patel, J. Johansen, and C. Chin, Observation of a degenerate Fermi gas trapped by a Bose-Einstein condensate, Phys. Rev. Lett. **119**, 233401 (2017).

[63] N. V. Corzo, J. Raskop, A. Chandra, A. S. Sheremet, B. Gouraud, and J. Laurat, Waveguide-coupled single collective excitation of atomic arrays, Nature (London) **566**, 359 (2019).

[64] G. A. Sinuco-Leon and B. M. Garraway, Radio-frequency dressed lattices for ultracold alkali atoms, New J. Phys. **17**, 053037 (2015).

[65] B. M. Garraway and H. Perrin, Recent developments in trapping and manipulation of atoms with adiabatic potentials, J. Phys. B: At. Mol. Opt. Phys. **49**, 172001 (2016).

[66] Y. He, L. Ji, Y. Wang, L. Qiu, J. Zhao, Y. Ma, X. Huang, S. Wu, and D. E. Chang, Geometric control of collective spontaneous emission, Phys. Rev. Lett. **125**, 213602 (2020).

[67] Y.-X. Zhang and K. Mølmer, Subradiant emission from regular atomic arrays: Universal scaling of decay rates from the generalized bloch theorem, Phys. Rev. Lett. **125**, 253601 (2020).